PROCEEDINGS OF SPIE

SPIEDigitalLibrary.org/conference-proceedings-of-spie

DMD-based spatially Fourier-encoded photoacoustic microscopy

Jinyang Liang, Liang Gao, Chiye Li, Lihong V. Wang

Jinyang Liang, Liang Gao, Chiye Li, Lihong V. Wang, "DMD-based spatially Fourier-encoded photoacoustic microscopy," Proc. SPIE 9323, Photons Plus Ultrasound: Imaging and Sensing 2015, 932324 (11 March 2015); doi: 10.1117/12.2076783

SPIE.

Event: SPIE BiOS, 2015, San Francisco, California, United States

DMD-based Spatially Fourier-encoded Photoacoustic Microscopy

Jinyang Liang, Liang Gao, Chiye Li, and Lihong V. Wang*
Optical Imaging Laboratory, Department of Biomedical Engineering, Washington University in St. Louis, Campus Box 1097, One Brookings Drive, St. Louis, Missouri 63130, USA

ABSTRACT

We present spatially Fourier-encoded photoacoustic microscopy using a digital micromirror device (DMD). The spatial fluence distribution of laser pulses is Fourier-encoded by the DMD, and a series of such encoded photoacoustic (PA) measurements enables decoding of the spatial distribution of optical absorption. By imaging a chromium target, we demonstrated the throughput and Fellgett advantages, which increased the PA signal-to-noise ratio (SNR) compared to raster scanning. The system was used to image two biological targets, a monolayer of red blood cells, and melanoma cells. The enhanced SNR benefited PA images by increasing the image's contrast-to-noise ratio and target identifiability.

Keywords: Photoacoustic imaging, Medical and biological imaging, Microscopy

1. INTRODUCTION

Optical-resolution photoacoustic microscopy (OR-PAM) [1-5], which provides label-free detection of endogenous contrasts of optical absorption, has been used in many medical and biological applications [6-10]. The photoacoustic (PA) signal amplitude in OR-PAM depends on both the optical absorption coefficient of the target and the local light fluence. A common way to achieve high specific optical absorption (J/m^3) is to increase the local light fluence. However, the light fluence cannot exceed the damage threshold. For biological tissues, the maximum light fluence is usually further restricted by the ANSI safety standard [11] for *in vivo* experiments. As the resultant PA signal is always mingled with random noise [12], a low PA signal-to-noise ratio (SNR) translates into a low contrast-to-noise ratio, which limits the visibility of features and the accuracy of functional imaging.

The SNR can be significantly improved by multiplexing. By dividing a target into sub-regions, each of which receives the same light intensity, more energy can be delivered to the target per laser pulse, yielding a throughput (Jacquinot) advantage over single-element illumination. The signal of each individual element can be recovered by decoding the measured signal series. If the measurement contains only signal-independent noise sources, *e.g.*, random thermal noise from an ultrasonic transducer or random electronic noise in the amplifiers, then multiplexing approaches may enhance the SNR of the recovered signal, which is known as the Fellgett advantage.

Fourier and Hadamard transformations are commonly used in multiplexing methods [13-18]. Both have been widely used as spectral encoding mechanisms in applied spectroscopy [14, 15] as well as in many imaging modalities [16-18]. Multiplexing approaches can also be implemented in the spatial domain. Recently, Rousseau and Blouin [19] demonstrated spatial Hadamard multiplexing in laser ultrasonics for the non-contact inspection of metal materials. A 2.8× SNR improvement was achieved by using a one-dimensional Hadamard mask with 31 elements, each with an area of 100×100 μm^2. However, this work cannot be readily implemented in microscopic biomedical imaging for two reasons. First, the utilization of the one-dimensional mask required scanning the target, resulting in a reduced imaging frame rate. Second, the lateral resolution (100 μm) was insufficient to distinguish micrometer-scale biological features.

In this paper, we present a spatially Fourier-encoded PAM (SFE-PAM) system using a digital micromirror device (DMD). This technique is inspired by the spectral Fourier-multiplexing method. The DMD was used as an optical encoder to produce time-domain discrete Fourier modulation patterns for each individual spatial element. Therefore, the SFE-PAM system can simultaneously deliver modulated light fluence to multiple locations of the target, thereby significantly improving the SNR of the PA signal over that of a single-element raster scan.

*Corresponding author: LHWANG@WUSTL.EDU.

Photons Plus Ultrasound: Imaging and Sensing 2015, edited by Alexander A. Oraevsky, Lihong V. Wang
Proc. of SPIE Vol. 9323, 932324 · © 2015 SPIE · CCC code: 1605-7422/15/$18
doi: 10.1117/12.2076783

2. THEORY

Herein we briefly review the Fourier multiplexing theory and derive the expected SNR enhancement for the SFE-PAM system [20]. A 2D area of the target is divided into N elements, each with an absorption coefficient of $\mu_a(n)$ $(n = 1, \ldots, N)$. A conventional raster scanning requires N element-by-element measurements. For the n-th element, the generated PA A-line detected by the ultrasonic transducer, $v_r(n,t)$, can be written as

$$v_r(n,t) = s_r(n,t) + e(n,t) \quad , \tag{1}$$

where

$$s_r(n,t) = \mu_a(n) F_0(n) \hat{v}(t) \quad . \tag{2}$$

Here, the subscript r denotes raster scanning, $s_r(n,t)$ represents the time-resolved PA signal, $F_0(n)$ represents the incident light fluence, and $\hat{v}(t)$ denotes the time-of-arrival PA signal generated by an absorber with a unit specific optical absorption [*i.e.*, $\mu_a(n) F_0(n) = 1$ J/m^3 or another chosen unit]. $e(n,t)$ represents the random noise from the ultrasonic transducer and signal amplifiers, and its standard deviation is denoted by σ_r.

To satisfy the Nyquist sampling requirement, 2(N+1) Fourier-encoded patterns are imaged into the target. The total PA signal amplitude is contributed by all N elements weighted by the Fourier-modulated light fluence. For the k-th measurement ($k = 0, \ldots, 2N+1$), the Fourier-encoded time-of-arrival PA signal, $V_f(k,t)$, can be written as

$$V_f(k,t) = \left(\sum_{n=1}^{N} \mu_a(n) F_0(n) \hat{F}_f(n,k) \right) \hat{v}(t) + e(k,t) \, , \tag{3}$$

where the subscript f denotes Fourier encoding. $\hat{F}_f(n,k) = 1 + \cos\left[\pi nk/(N+1)\right]$ describes the fact that the laser pulse energy of each spatial element n is modulated by a distinct frequency associated with the measurement index k (Fig. 1). The Fourier-encoded time-of-arrival PA signals from successive 2(N+1) measurements are stacked to form a signal sequence.

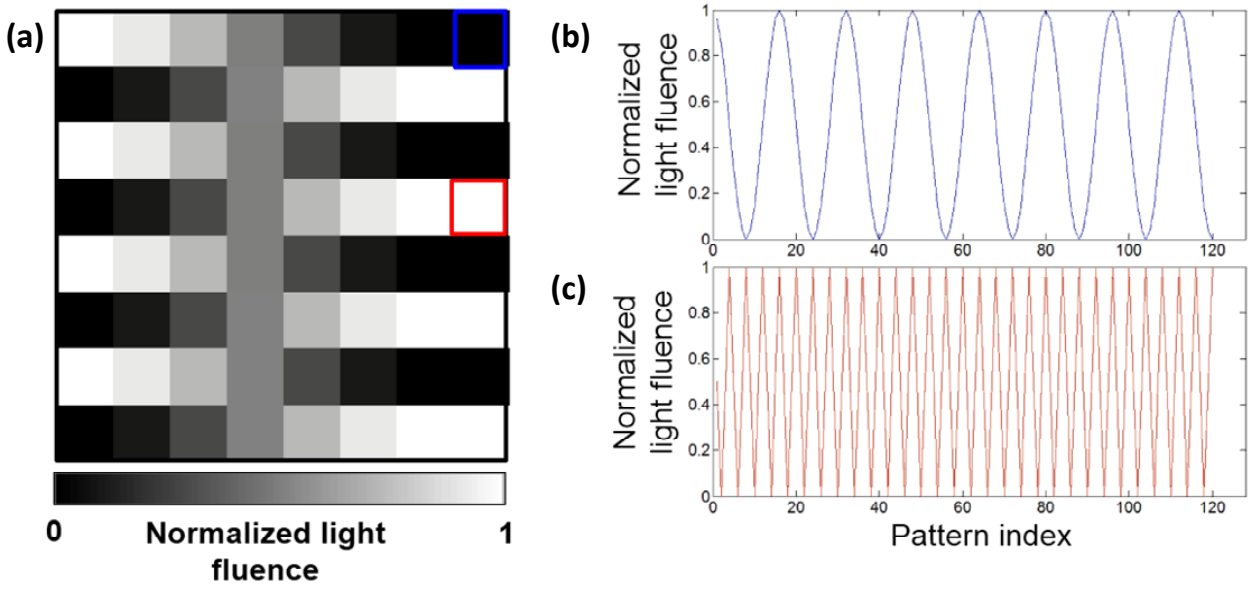

Fig. 1 Principle of Fourier-encoded illumination. A representative Fourier-encoded illumination pattern is shown in (a). The normalized light fluence of elements [blue box and red box in (a)] versus illumination pattern index is shown in (b) and (c).

This sequence is then decoded using the inverse Fourier transformation, which extracts the magnitude at each modulation frequency. The Fourier-decoded PA A-line, $v_f(m,t)$, can be written as

$$v_f(m,t) = s_f(m,t) + \varepsilon(m,t), m = -N, \ldots, N+1, \tag{4}$$

where

$$s_f(m,t) = \frac{1}{2(N+1)} \sum_{k=0}^{2N+1} \left\{ \left(\sum_{n=1}^{N} \mu_a(n) F_0(n) \hat{F}_f(n,k) \right) \hat{v}(t) \right\} \exp\left(i\pi \frac{mk}{N+1} \right), \tag{5}$$

and

$$\varepsilon(m,t) = \frac{1}{2(N+1)} \sum_{k=0}^{2N+1} e(k,t) \exp\left(i\pi \frac{mk}{N+1} \right). \tag{6}$$

Here, Eqs. (5) and (6) represent the signal and noise in the decoded PA A-line. N elements ($m = 1,\ldots,N$) from Eq. (5) form an image, given by

$$s_f(m,t) = \frac{1}{2} \sum_{n=1}^{N} \mu_a(n) F_0(n) \delta_{mn} \hat{v}(t), \tag{7}$$

where δ_{mn} is the Kronecker delta function. Equation (7) shows that each recovered element contains only half the value of the corresponding absorption coefficient, compared to the raster scan measurement. The PA amplitudes of raster-scanned and Fourier-decoded PA A-lines are calculated by taking the absolute value of the Hilbert transforms of $s_r(n,t)$ and $s_f(n,t)$, respectively. Their ratio is found to be

$$\frac{\left| H\{s_f(n,t)\} \right|}{\left| H\{s_r(n,t)\} \right|} = \frac{1}{2}, \tag{8}$$

where $H\{\}$ denotes the Hilbert transformation.

In addition, we compared the standard deviation of the PA signal amplitude in raster-scanned and Fourier-decoded PA A-lines. The signal's standard deviation in the Fourier-decoded PA A-line, σ_f, is derived from Eq. (6):

$$\sigma_f = \frac{1}{\sqrt{2(N+1)}} \sigma_r. \tag{9}$$

However, to compensate for the unequal numbers of measurements, it is necessary to average the raster scan over two measurements because the Fourier encoding requires twice as many measurements as the raster scanning in general for $N >> 1$. This reduces the standard deviation in the raster-scanned PA A-line by a factor of $\sqrt{2}$, *i.e.*, $\sigma_r' = \sigma_r / \sqrt{2}$. Equation (9) becomes

$$\sigma_f = \frac{1}{\sqrt{N+1}} \sigma_r'. \tag{10}$$

Thus, compared to conventional raster scanning PAM, the Fourier encoding method suppresses the noise by a factor of $\sqrt{N+1}$.

The Fellgett advantage η is defined as the ratio of the SNR of the decoded PA A-line, $SNR_f(n,t) \equiv \left| H\{s_f(n,t)\} \right| / \sigma_f$, to that of the raster-scanned PA A-line, $SNR_r(n,t) \equiv \left| H\{s_r(n,t)\} \right| / \sigma_r'$. Combining Eqs. (8) and (10) gives

$$\eta \equiv \frac{SNR_f(n,t)}{SNR_r(n,t)} = \frac{\sqrt{N+1}}{2}. \tag{11}$$

3. SYSTEM

The DMD-based SFE-PAM system (Fig. 2) [20] employs a Nd:YVO_4 laser (SPOT 10-200-532, $\lambda = 532$ nm, Elforlight) as the illumination source. The incident laser pulses have a 2 ns pulse duration with a repetition rate of 10 kHz. The pulse energy is monitored by a photodiode detector (SM05PD1A, Thorlabs) to compensate for energy fluctuation. After expansion and collimation, the laser pulses impinge on the DMD (Discovery 4100, Texas Instruments) at an incident angle of 24° with respect to the surface normal. For each individual Fourier-modulation pattern, we use the two-dimensional Floyd-Steinberg error diffusion algorithm [21] to generate the corresponding DMD pattern, which is then imaged onto the target through a system consisting of two 4*f* telescopes. Due to the limited spatial bandwidth of the imaging system, binary DMD patterns are converted to continuous grayscale images on the target. A 50 MHz ultrasonic transducer (V214-BB-RM, Olympus NDT Panametrics), placed confocally with the optical objective lens (Olympus, LUCPlanFLN 40×/0.60), is used to detect the PA signal. To fit the acoustic focal size of the transducer, the illumination field of view is set to be 35×35 μm^2, with a lateral resolution of ~3.5 μm [22]. The optically determined lateral resolution limits the imaging depth to ~1 mm [4].

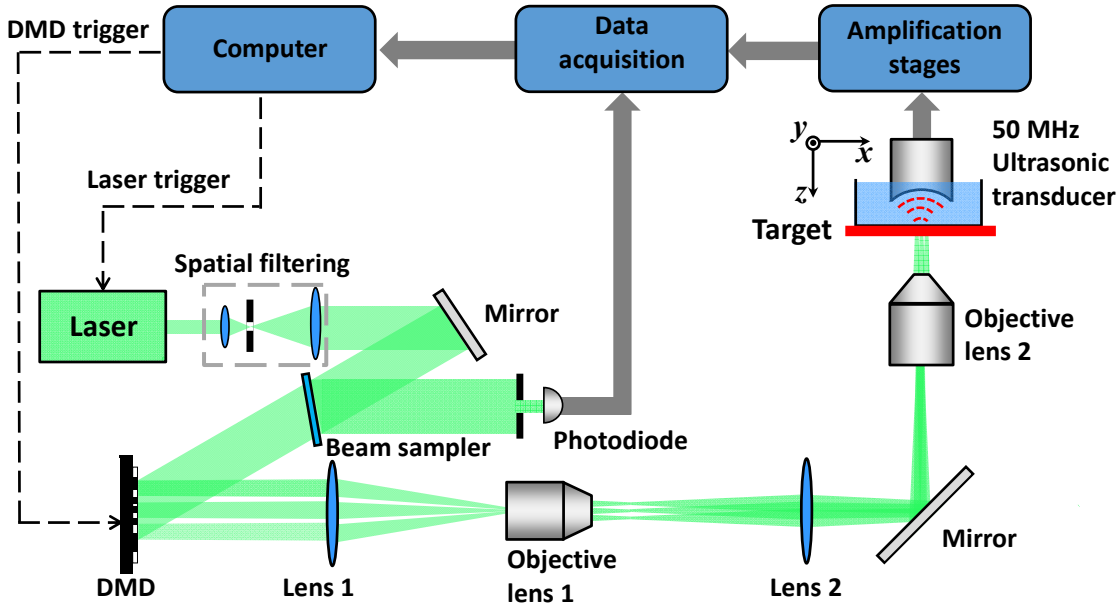

Fig. 2. Schematic overview of the spatially Fourier-encoded photoacoustic microscopy system (not to scale). DMD, digital micromirror device; Objective lens 1 (Mitutoyo, M PLAN APO 10×/0.28); Objective lens 2 (Olympus, LUCPlanFLN 40×/0.60).

4. RESULTS

To demonstrate spatial Fourier-encoding in PAM, we first imaged a chromium target of the letters "WU", made in-house by vacuum-deposition on a microscope coverslip substrate [Fig. 3(a)]. The illumination field of view was evenly divided into 8×8 elements, in which n = 1,…,63 elements were used for Fourier encoding. At the DMD face, each element corresponds to 96×96 micromirrors. According to Eq. (11), the expected SNR enhancement is 4×. The average pulse energy was set to be 1.1 nJ per element. Compared to raster scanning, the spatial Fourier encoding was experimentally shown to significantly increase the SNR of the data. Representative results of $v_r(n,t)$ and $V_f(m,t)$ are compared in Fig. 3(b), and show that the Fourier-encoded PA time-of-arrival signal has an 8× better SNR.

After Fourier decoding, a volumetric image of the target's optical absorption was produced by allocating each individual PA A-line in the stack to the corresponding spatial element position. Then this volumetric 3D image was rendered as a 2D maximum amplitude

projection (MAP) image along the depth direction. The PA image of the letters "WU" demonstrates that the Fourier encoding significantly enhanced image quality compared to the raster scanning [Fig. 3(c)].

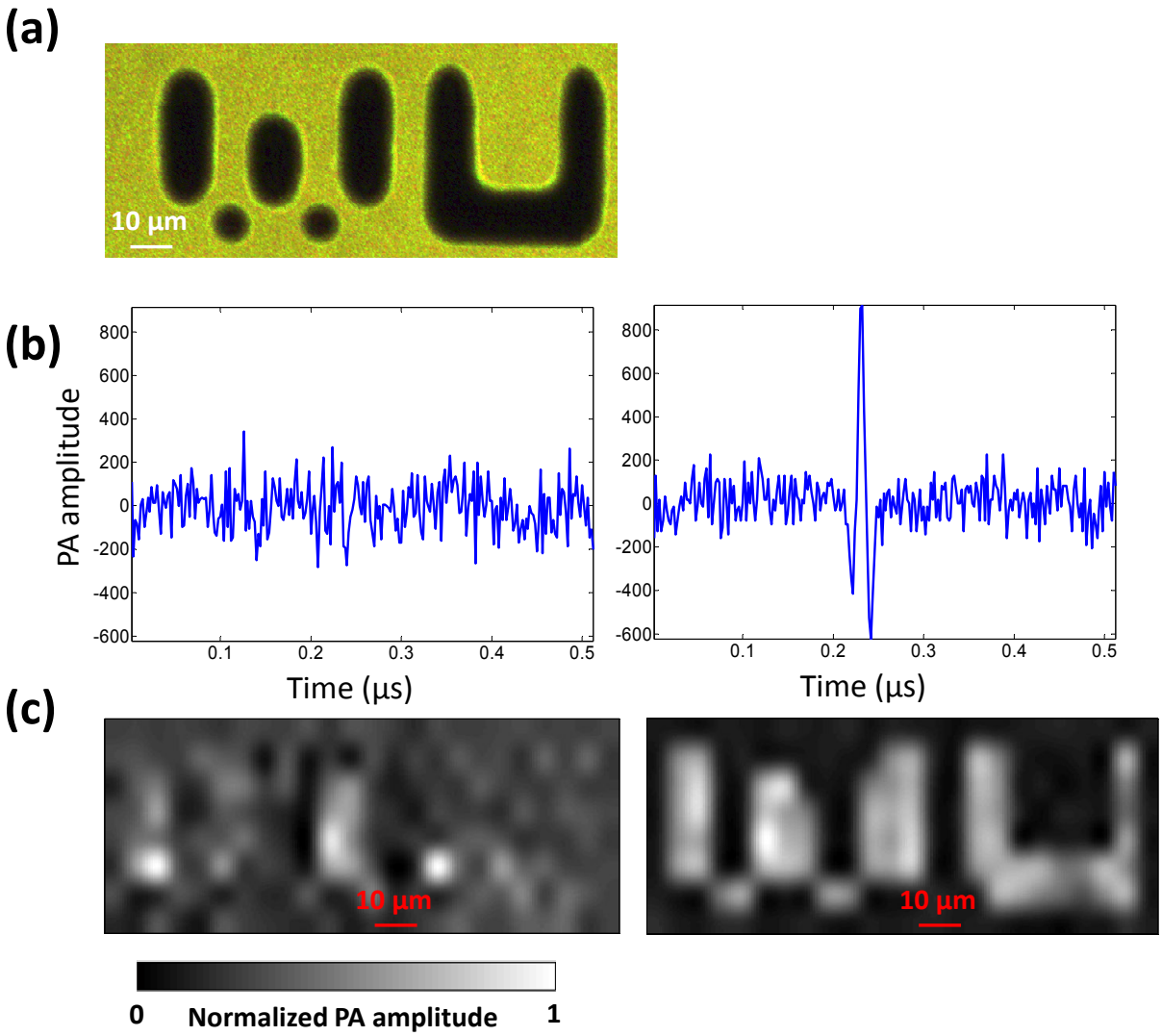

Fig. 3 (a) A transmissive photograph of the "WU" target. (b) Comparison of PA time-of-arrival signals from raster scanning (left) and Fourier encoding (right). (c) PA images of "WU" acquired by raster scanning (left) and Fourier encoding (right).

To test the SFE-PAM system performance with biological contrasts, we imaged melanoma cells and red blood cells (RBCs) (Fig. 4). The average pulse energy was set to be 2.8 nJ per element. In both cases, while no features could be identified using the raster scanning, the cellular shape was clearly revealed by the PA image obtained by the Fourier encoding. These results demonstrated that the PA image quality was considerably improved by using the Fourier-encoding method. Although implemented in OR-PAM, the conceptual design of spatial Fourier encoding is applicable to many other imaging modalities, *e.g.*, fluorescent microscopy. Compared to traditional interferometry-based Fourier modulation approaches, the present approach uses a DMD as a spatial Fourier encoder. Avoiding a moving reference mirror, the SFE-PAM system acquires images without mechanical movement, making the system more stable for practical applications. In comparison to a laser illumination array [23], the present system requires only a single laser source and gives users the flexibility to control the number of spatial elements used according to the application.

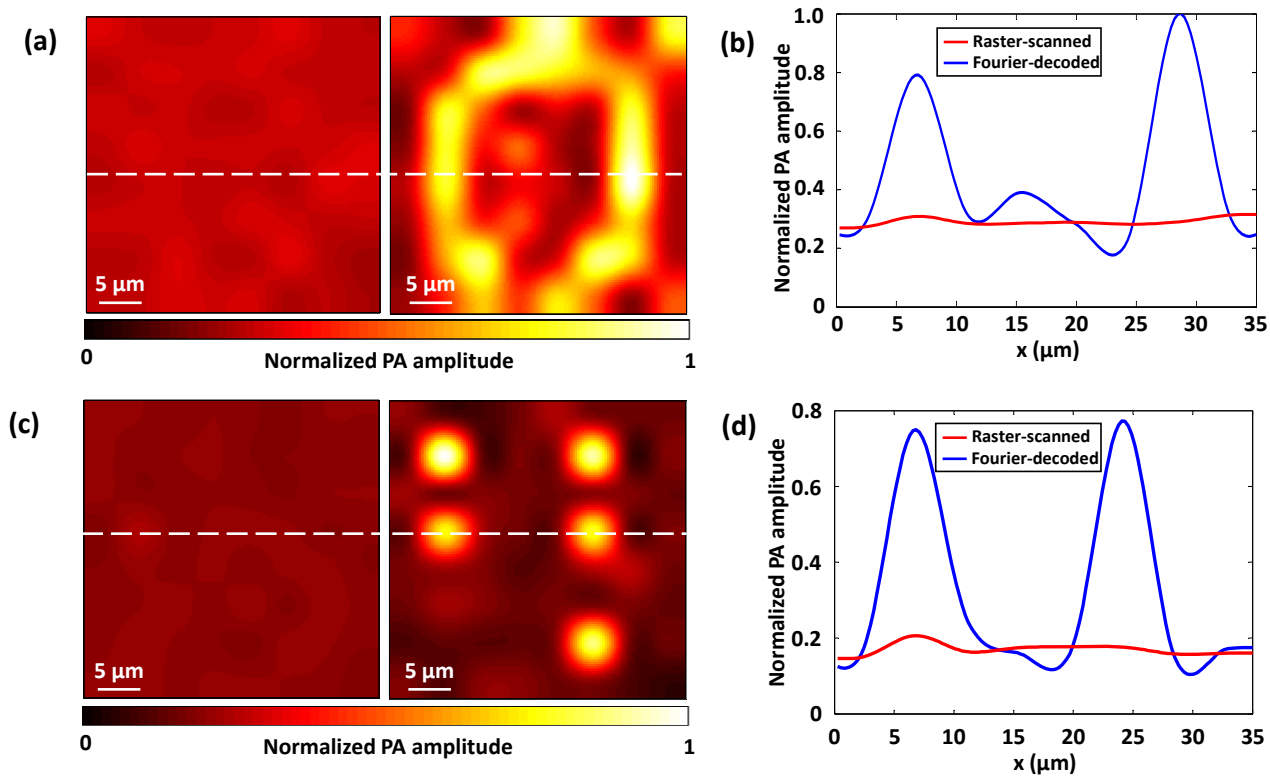

Fig. 4. Demonstration of spatial Fourier-encoding method in biological targets. PA images of a melanoma cell (a) acquired by raster scanning [left image in (a)] and Fourier encoding [right image in (a)]. The PA amplitude from the white dashed line in (a) is compared in (b). Monolayer RBCs were also imaged using raster scanning [left in (c)] and Fourier encoding [right in (c)]. The PA amplitude from the white dashed line in (c) is compared in (d).

5. SUMMARY

In summary, we report the first experimental demonstration of a SFE-PAM system based on a DMD, which modulates the spatial light distribution of the laser beam. Each spatial element of the target is illuminated by modulated light fluence with a different frequency. The spatial optical absorption distribution is recovered by decoding a series of Fourier-encoded PA measurements. Compared to raster scanning with the same number of measurements, the SFE-PAM system enables more energy-efficient delivery of the laser illumination. In addition, this system possesses the Fellgett advantage, in terms of PA SNR, in the Fourier-decoded PA A-lines. The enhanced SNR benefits PA images by increasing the image's contrast-to-noise ratio and target identifiability. The SFE-PAM system is an attractive tool for the accurate PA measurement of biological targets with low optical absorption coefficients or low damage thresholds.

ACKNOWLEDGMENTS

The authors thank Dr. Lijun Ma, Yong Zhou, Dr. Chi Zhang, and Lei Li for helpful discussions, and Professor James Ballard for close reading of the manuscript. This work was sponsored in part by National Institutes of Health grants DP1 EB016986 (NIH Director's Pioneer Award), R01CA134539, R01CA157277, and R01 CA159959. L. W. has a financial interest in Microphotoacoustics, Inc. and Endra, Inc., which, however, did not support this work.

REFERENCES

[1] Maslov, K., Zhang, H. F., Hu, S., and Wang, L. V., "Optical-resolution photoacoustic microscopy for in vivo imaging of single capillaries," Opt. Lett., 33(9), 929-931 (2008).

[2] Liang, J., Zhou, Y., Winkler, A. W., Wang, L., Maslov, K. I., Li, C., and Wang, L. V., "Random-access optical-resolution photoacoustic microscopy using a digital micromirror device," Opt. Lett., 38(15), 2683-2686 (2013).

[3] Hai, P., Yao, J., Maslov, K. I., Zhou, Y., and Wang, L. V., "Near-infrared optical-resolution photoacoustic microscopy," Opt. Lett., 39(17), 5192-5195 (2014).

[4] Wang, L. V., and Hu, S., "Photoacoustic Tomography: In Vivo Imaging from Organelles to Organs," Science, 335(6075), 1458-1462 (2012).

[5] Yeh, C., Soetikno, B., Hu, S., Maslov, K. I., and Wang, L. V., "Microvascular quantification based on contour-scanning photoacoustic microscopy," BIOMEDO, 19(9), 096011-096011 (2014).

[6] Paproski, R. J., Forbrich, A. E., Wachowicz, K., Hitt, M. M., and Zemp, R. J., "Tyrosinase as a dual reporter gene for both photoacoustic and magnetic resonance imaging," Biomed. Opt. Express, 2(4), 771-780 (2011).

[7] Jiao, S., Jiang, M., Hu, J., Fawzi, A., Zhou, Q., Shung, K. K., Puliafito, C. A., and Zhang, H. F., "Photoacoustic ophthalmoscopy for in vivo retinal imaging," Opt. Express, 18(4), 3967-3972 (2010).

[8] Li, R., Slipchenko, M. N., Wang, P., and Cheng, J.-X., "Compact high power barium nitrite crystal-based Raman laser at 1197 nm for photoacoustic imaging of fat," Journal of Biomedical Optics, 18(4), 040502-040502 (2013).

[9] Gao, L., Wang, L., Li, C., Liu, Y., Ke, H., Zhang, C., and Wang, L. V., "Single-cell photoacoustic thermometry," BIOMEDO, 18(2), 026003-026003 (2013).

[10] Liang, J., Zhou, Y., Maslov, K. I., and Wang, L. V., "Cross-correlation-based transverse flow measurements using optical resolution photoacoustic microscopy with a digital micromirror device," BIOMEDO, 18(9), 096004-096004 (2013).

[11] "American National Standard for Safe Use of Lasers ANSI Z136.1 – 2007," ((Laser Institute of America, Orlando, Florida, 2007)).

[12] Mathangi, S., Konstantin, M., Hao, F. Z., George, S., and Lihong, V. W., "Limitations of quantitative photoacoustic measurements of blood oxygenation in small vessels," Physics in Medicine and Biology, 52(5), 1349 (2007).

[13] Graff, D. K., "Fourier and Hadamard: transforms in spectroscopy," Journal of chemical education, 72(4), 304 (1995).

[14] Griffiths, P. R., and De Haseth, J. A., [Fourier transform infrared spectrometry] John Wiley & Sons, (2007).

[15] Hammaker, R. M., Bohlke, A. P., Jarvis, J. M., Tate, J. D., White, J. S., Paukstelis, J. V., and Fateley, W. G., "Recent developments in Hadamard transform Raman spectrometry." 124-134.

[16] Eberhardt, K. W., Hunkeler, A., Meier, U., Tharian, J., Mouaziz, S., Boero, G., Brugger, J., and Meier, B. H., "Two-dimensional magnetic resonance force microscopy using full-volume Fourier and Hadamard encoding," Physical Review B, 78(21), 214401 (2008).

[17] Wang, Y., Maslov, K., and Wang, L. V., "Spectrally encoded photoacoustic microscopy using a digital mirror device," BIOMEDO, 17(6), 0660201-0660205 (2012).

[18] Hanley, Q., Verveer, P., Arndt-Jovin, D., and Jovin, T., "Three-dimensional spectral imaging by Hadamard transform spectroscopy in a programmable array microscope," Journal of microscopy, 197(1), 5-14 (2000).

[19] Rousseau, G., and Blouin, A., "Hadamard multiplexing in laser ultrasonics," Opt. Express, 20(23), 25798-25816 (2012).

[20] Liang, J., Gao, L., Li, C., and Wang, L. V., "Spatially Fourier-encoded photoacoustic microscopy using a digital micromirror device," Opt. Lett., 39(3), 430-433 (2014).

[21] Liang, J., Kohn, J. R. N., Becker, M. F., and Heinzen, D. J., "1.5% root-mean-square flat-intensity laser beam formed using a binary-amplitude spatial light modulator," Appl. Opt., 48(10), 1955-1962 (2009).

[22] Liang, J., Zhou, Y., Winkler, A. W., Wang, L., Maslov, K. I., Li, C., and Wang, L. V., "Random-access optical-resolution photoacoustic microscopy using a digital micromirror device," Opt. Lett., 38(15), 2683-2686 (2013).

[23] Steckenrider, J. S., Murray, T. W., Wagner, J. W., and John B. Deaton, J., "Sensitivity enhancement in laser ultrasonics using a versatile laser array system," The Journal of the Acoustical Society of America, 97(1), 273-279 (1995).